Cochlear Implant Artifacts Removal in EEG-Based Objective Auditory Rehabilitation Assessment

Qi Zheng, Yubo Wu, Jianing Zhu, Leqiang Cao, Yanru Bai, and Guangjian Ni, *Member, IEEE*

***Abstract*— Cochlear implant (CI) is a neural prosthesis that can restore hearing for patients with severe to profound hearing loss. Observed variability in auditory rehabilitation outcomes following cochlear implantation may be due to cerebral reorganization. Electroencephalography (EEG), favored for its CI compatibility and non-invasiveness, has become a staple in clinical objective assessments of cerebral plasticity post-implantation. However, the electrical activity of CI distorts neural responses, and EEG susceptibility to these artifacts presents significant challenges in obtaining reliable neural responses. Despite the use of various artifact removal techniques in previous studies, the automatic identification and reduction of CI artifacts while minimizing information loss or damage remains a pressing issue in objectively assessing advanced auditory functions in CI recipients. To address this problem, we propose an approach that combines machine learning algorithms—specifically, Support Vector Machines (SVM)—along with Independent Component Analysis (ICA) and Ensemble Empirical Mode Decomposition (EEMD) to automatically detect and minimize electrical artifacts in EEG data. The innovation of this research is the automatic detection of CI artifacts using the temporal properties of EEG signals. By applying EEMD and ICA, we can process and remove the identified CI artifacts from the affected EEG channels, yielding a refined signal. Comparative analysis in the temporal, frequency, and spatial domains suggests that the corrected EEG recordings of CI recipients closely align with those of peers with normal hearing, signifying the restoration of reliable neural responses across the entire scalp while eliminating CI artifacts.**

***Index Terms*— Cochlear implant, artifact removal, electroencephalography (EEG), support vector machines SVM, ensemble empirical mode decomposition (EEMD).**

Manuscript received 5 January 2024; revised 21 May 2024; accepted 29 July 2024. Date of publication 5 August 2024; date of current version 12 August 2024. This work was supported in part by the National Key Research and Development Program of China under Grant 2023YFF1203500 and in part by the National Natural Science Foundation of China under Grant 81971698. *(Qi Zheng and Yubo Wu contributed equally to this work.) (Corresponding author: Guangjian Ni.)*

This work involved human subjects or animals in its research. Approval of all ethical and experimental procedures and protocols was granted by the Ethics Committee of Tianjin University under Application No. TJUE-2023-207.

Qi Zheng, Jianing Zhu, and Leqiang Cao are with the Academy of Medical Engineering and Translational Medicine and the Department of Biomedical Engineering, College of Precision Instruments and Optoelectronics Engineering, Tianjin University, Tianjin 300072, China (e-mail: zhengqi0229@tju.edu.cn; jianing_zhu@tju.edu.cn; caolq200010@163.com).

Yubo Wu is with the Academy of Medical Engineering and Translational Medicine, Tianjin University, Tianjin 300072, China (e-mail: 1023235009@tju.edu.cn).

Yanru Bai is with the Academy of Medical Engineering and Translational Medicine, Tianjin University, Tianjin 300072, China, and also with the Haihe Laboratory of Brain-Computer Interaction and Human-Machine Integration, Tianjin 300392, China (e-mail: yr56_bai@tju.edu.cn).

Guangjian Ni is with the Academy of Medical Engineering and Translational Medicine and the Department of Biomedical Engineering, College of Precision Instruments and Optoelectronics Engineering, Tianjin University, Tianjin 300072, China, and also with the Haihe Laboratory of Brain-Computer Interaction and Human-Machine Integration, Tianjin 300392, China (e-mail: niguangjian@tju.edu.cn).

Digital Object Identifier 10.1109/TNSRE.2024.3438149

I. Introduction

COCHLEAR implants (CI) are the most effective intervention for severe to profound hearing loss. Over one million individuals with hearing impairments globally have regained functional auditory perception with the aid of CIs, approximately 50% of whom are children [1]. Post-implantation, the clinicians are required to regularly calibrate the threshold levels (T values) and comfortable levels (C values) settings in accordance with auditory assessment test results [2]. Accurate postoperative auditory evaluations are crucial for guiding clinicians in developing treatment plans. Currently, clinical assessments of hearing post-CI implantation predominantly rely on speech-based or non-speech behavioral tests [3], [4], [5]. However, the accuracy of these behavioral results can be greatly affected during the period when CI recipients are acclimating to newly introduced electrical auditory speech signals after device activation. It underlines the importance of objective methods that assess neural responses without patient cooperation [6].

Electroencephalography (EEG) provides researchers and clinicians with a direct observation method of neuron responses to auditory stimuli with high temporal resolution. Cortical Auditory Evoked Potentials (CAEP) and Mismatch Negativity (MMN) hold significant clinical potential for evaluating advanced auditory function recovery in CI users and are considered biomarkers for their auditory rehabilitation [7], [8], [9]. With advancements in neuroscience research, an increasing focus is placed on investigating brain plasticity in CI users. Functional Magnetic Resonance Imaging (fMRI)

and Positron Emission Tomography (PET) are robust tools for studying brain structure and function. However, the strong electromagnetic fields of fMRI are incompatible with CI, and PET requires radioactive tracers to track brain activity [10]. EEG emerges as the most suitable objective method for exploring brain plasticity in CI users, especially during the phase of learning new input sounds. Multidimensional objective indices based on EEG's time-frequency-spatial domains can provide more information on the neural mechanisms during auditory rehabilitation in CI users, enhancing our understanding of cerebral functional reorganization following new auditory input.

Nevertheless, EEG recordings are easily contaminated by electromagnetic interference from CIs [11], with simultaneous recording of CI artifacts. These artifacts sometimes exceed the neural activity of interest by several orders of magnitude. CI artifacts are often time-locked with brain responses to sound stimuli, severely distorting the neural responses induced by auditory stimuli [12], with relevant features often drowned in CI noise. Such interference obscures researchers' targeted features, particularly when investigating auditory rehabilitation biomarkers in CI users. More crucially, CI artifacts pose challenges in studies investigating auditory plasticity in CI users based on whole-head EEG signals. Therefore, further developing studies that extract neural activity changes in CI users from EEG and eliminate CI artifacts' interference with whole-head signals is of paramount importance.

The researchers have employed various preprocessing strategies to reduce CI artifacts. Initially, when focusing only on CAEP components recorded at the midline, a re-referencing technique was proposed to maximize the signal-to-noise ratio [13]. For unilateral CI users, re-referencing to the mastoid on the opposite side of the implant and for bilateral CI users, to the tip of the nose. Some have also attempted to minimize artifacts by disconnecting or removing electrodes proximal to the CI during experimentation or preprocessing. Yet, these methods do not fully mitigate CI artifacts. and can lead to considerable data loss, limiting the exploration of auditory plasticity post-implantation and negatively impacting whole-head signal neural source estimation. Hofmann and Wouters proposed a linear interpolation method to attenuate CI artifacts [14], which Deprez et al. found to be effective only for electrodes on the side opposite the implant and only when the interval between stimulus pulses is longer than the duration of the pulse artifact. Later, Mc Laughlin et al. proposed a single-channel artifact attenuation method, weakening high-frequency and direct-current CI artifacts in the Late Auditory Evoked Potentials (LAEPs) of 22 adult CI subjects [15]. However, when BinKhamis et al. used linear interpolation and template subtraction, they obtained clean data from only 2 out of 12 CI users' EEG recordings [16]. Increasingly, studies use Independent Component Analysis (ICA) to remove CI artifact components. ICA, part of blind source separation [17], has been widely applied in EEG preprocessing for artifact removal, such as electrooculogram (EOG), electromyography (EMG), electrocardiogram (ECG), and head movements [18], [19]. However, CI artifacts often mix with other neural activities in the same component, and the actual Independent Components (ICs) related to CI artifacts can number in the dozens [20]. Removing too many CI-related ICs can directly distort whole-head signals while removing too few can affect the accuracy of source estimation in brain plasticity studies.

A growing body of electroencephalographic (EEG) research is utilizing more ecological stimuli, such as speech stimuli, to examine cerebral functional reorganization. However, the limitations of using only ICA become apparent with complex stimuli, making it difficult to eliminate CI artifacts completely. Each CI manufacturer has its own coding strategy, resulting in different CI artifacts in EEG recordings. Additionally, due to individual differences and slight positional shifts of the EEG cap, the number of leads with residual CI artifacts varies. Moreover, for CI users, the characteristics of stimulus-evoked components are constantly evolving during the rehabilitation phase as they acclimate to new auditory inputs post-implantation. Investigating cerebral plasticity is pivotal to comprehending the auditory function reconstruction post-CI implantation. Consequently, we have developed a semi-automatic method that effectively eliminates CI artifacts induced by different auditory stimuli from whole-lead EEG signals. This method minimizes information loss while reducing artifacts with minimal supervision, providing an artifact elimination tool for clinical assessment on cerebral plasticity in CI users.

In this investigation, we conducted artifact elimination experiments on high-density EEG data from CI patients, aiming to validate the direct applicability of the artifact elimination tool in clinical evaluations of advanced auditory functions. Given the scarcity of literature on CI artifacts removal in EEG recordings and the limited priori knowledge of engineering techniques among clinicians, we devised an automated model to identify artifact characteristics and segregate channels affected by CI artifacts in high-density EEG. The implemented machine learning approach yielded a commendable accuracy rate (approximately 95%). For processing channels contaminated with CI artifacts, we utilized EEMD-ICA method, adept at adjusting to the data's inherent nonlinearity and non-stationarity. And guidelines are provided for removing ICs containing only CI artifacts. This method ensures thorough artifact removal while maintaining data integrity, accurately mirroring the characteristics of the original neural signals, and ultimately resulting in corrected EEG recordings.

II. Material and Methods

A. Dataset

Data collection occurred in an electromagnetic anechoic chamber over three distinct sessions, each utilizing a different auditory stimulus: pure tones, syllables, and tonal sounds. The objective was to assess the auditory perceptual abilities of CI recipients in response to a range of speech complexities post-implantation. Utilizing an auditory oddball paradigm, the study focused on a singular deviant stimulus during each session. Two auditory stimuli were presented: a 1 kHz tone (200 ms) (S) and a 1.5 kHz tone (200 ms) (D), the Mandarin syllables "ba" (305 ms) (S) and "pa" (305 ms) (D), and the Mandarin tones "bā" (305 ms) (S) and "bà" (305 ms) (D), with 'S' signifying the standard and 'D' the deviant. The stimuli

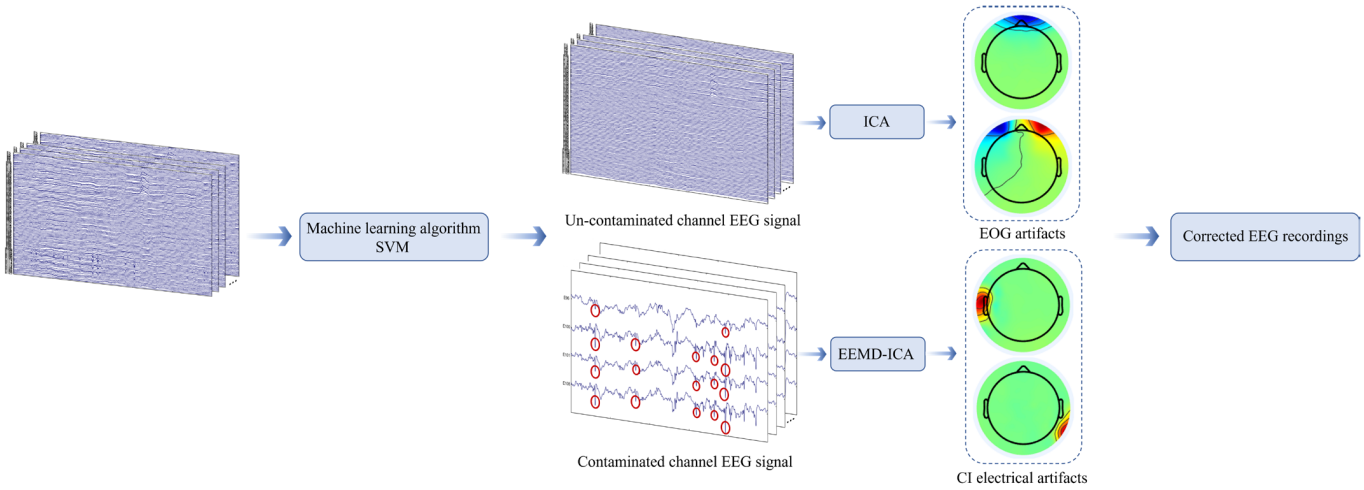

Fig. 1. CI Artifact Removal Algorithm Overview. Following initial preprocessing, EEG data are classified into two categories using SVM: channels unaffected and affected by CI artifacts. Channels free from CI artifacts undergo removal of common artifacts such as EOG, EMG, ECG artifacts. Those impacted by CI are processed using the EEMD-ICA algorithm to extract CI artifacts, resulting in a refined full-lead EEG signal.

occurred at random intervals ranging from 600 to 800 milliseconds. Sessions commenced with an initial sequence of 10 standard stimuli, succeeded by 1000 trials comprising 85% standard and 15% deviant stimuli. Detailed experimental protocols can be accessed in published papers [21]. In this study, EEG data were gathered from 66 children with CI, aged 3 to 7 years, and 25 normal hearing peers. The dataset includes 23 recordings elicited by pure tone stimuli, 16 by syllable stimuli, and 27 by tonal stimuli. Participants were engaged in passive listening to the auditory sequences while viewing their preferred silent cartoons. Following sound field calibration, auditory inputs were delivered at 70 dB SPL to guarantee detectability by all participants.

Electroencephalogram (EEG) data were captured using a 128-channel saline electrode cap, part of the Geodesic Sensor Net (GSN), amplified by a Net Amps 400 amplifier, and recorded at a sampling rate of 1kHz. The electrode array adhered to the standard international 10-20 system placements, supplemented with additional sites, incorporating the reference electrode at Cz and the ground electrode situated between CPz and Pz.

B. Conventional Data Preprocessing

The experimental data underwent digital band-pass filtering within the 0.1-30 Hz range, supplemented with a 50 Hz notch filter to attenuate low-frequency drift and high-frequency noise. The filtered continuous EEG data were then divided into epochs ranging from 100 ms before the stimulus to 500 ms after, with each epoch undergoing baseline correction. Epochs exhibiting electrical activity surpassing 100 microvolts were excluded. Comparative studies on the performance of ICA algorithms demonstrated that Infomax had a minimal negative effect on EEG recordings with CI artifacts during the noise reduction process [22], [23]. Consequently, the Infomax algorithm was employed to compute ICs, with the ADJUST algorithm subsequently setting the threshold at 0.9 to facilitate the automatic elimination of EOG, EMG, ECG artifacts. During this phase, CI artifacts were not processed.

C. Artifact Processing Methods

Analysis of single-lead signals indicated substantial distortion in electrodes proximal to the CI external device, attributed to CI electrical activity. It was observed that the interference in electrode recordings decreased as the distance from the CI implant increased. Moreover, electrodes situated further from the CI implant demonstrated a higher signal-to-noise ratio and clearer event-related potential (ERP) features. In addition, up to dozens of CI-related ICs were identified, encompassing those exclusively composed of CI artifacts and others combining CI artifacts with pertinent physiological activities. Completely removing all CI-related ICs risked distorting relevant physiological activities in other leads. In contrast, selectively removing components containing only CI artifacts left residual artifacts in CI-affected leads, compromising the analysis of neural plasticity.

To address this challenge, the preliminarily preprocessed EEG data were classified into two categories using SVM: leads not influenced by CI contamination and those that were. The unaffected leads underwent component removal for disturbances such as EOG, EMG, ECG artifacts in the previous phase, while the affected leads had CI components extracted using the EEMD-ICA algorithm. This approach yielded artifact-corrected whole-lead signals, as depicted in Figure 1. The detailed methodology is outlined subsequently.

1) CI Artifacts in EEG Recordings: The morphology of CI artifacts in EEG recordings exhibits variation across several factors [24]. The most noteworthy thing is that these artifacts tend to mirror the envelope contours of auditory stimuli. Speech stimuli, with their array of time-varying frequencies, produce more intricate artifacts compared to pure tones. In the cochlear implant (CI) dataset presented in this study, similar evidence was observed, yet artifacts did not align precisely with the auditory stimulus envelope, as illustrated in Figure 2. Figures 2A and 2B respectively illustrate the envelopes of Mandarin tones “bā” (first tone) and “bà” (fourth tone), accompanied by the resultant CI artifacts induced by these stimuli. Although CI artifacts generally reflected the trends

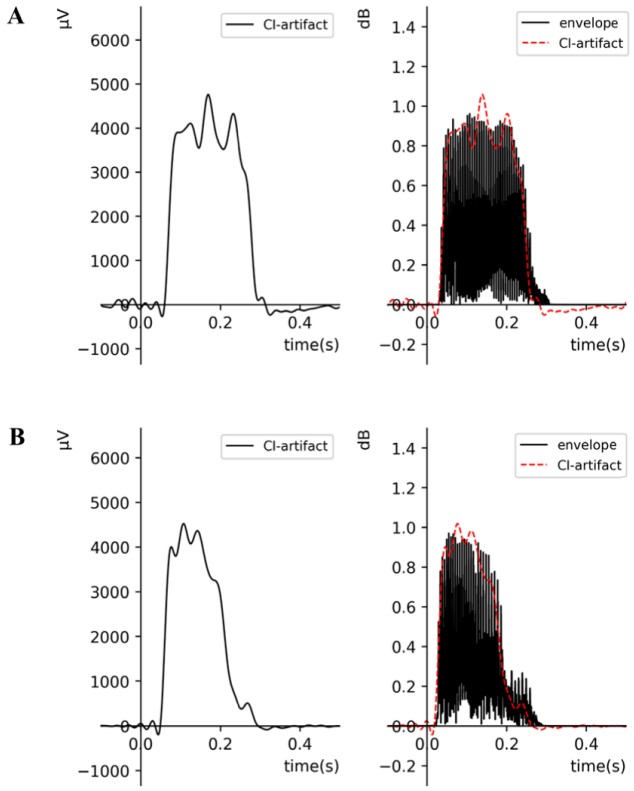

Fig. 2. Envelope Comparison between CI Artifacts and Stimulus Speech. Panel A illustrates the envelope of the Mandarin tone "bā" and its associated CI artifact, whereas Panel B demonstrates the envelope for the tone "bà" and its corresponding CI artifact. CI artifacts mimic the envelope patterns of the speech stimuli but are not perfectly aligned.

of the speech stimuli, the reason they were not precisely aligned may be due to artifact distortion at 1kHz sampling rate [25]. However, a prevalent characteristic observed in EEG recordings across various speech stimuli is that electrodes proximal to the CI manifest artifacts. Electrodes that are further yet still impacted by electrical artifacts demonstrate spikes exceeding the magnitude of the neural activity adjacent to the ERP components. It is argued that dependence on the speech stimulus envelope for precise identification of all signals contaminated by CI in speech stimuli may not be effective in clinical objective evaluations. To meet the clinical demand for a swift assessment of patients' auditory perceptual abilities with different speech stimuli, this study proposes an SVM algorithm-based method for the automatic classification of CI-contaminated EEG recordings, alongside a developed model for isolating CI-contaminated channels in EEG recordings under different speech stimuli.

2) Automatic Classification of CI-Contaminated EEG Recordings Using SVM: Given the limited literature and consensus on the automatic identification of CI artifacts, experts initially visually inspected and identified 1,175 out of 8,448 leads (66 subjects * 128 leads) as CI artifact contaminated. This was followed by training a SVM classifier to distinguish between CI-affected and unaffected leads, facilitating the automatic categorization of CI-contaminated EEG records in pediatric datasets.

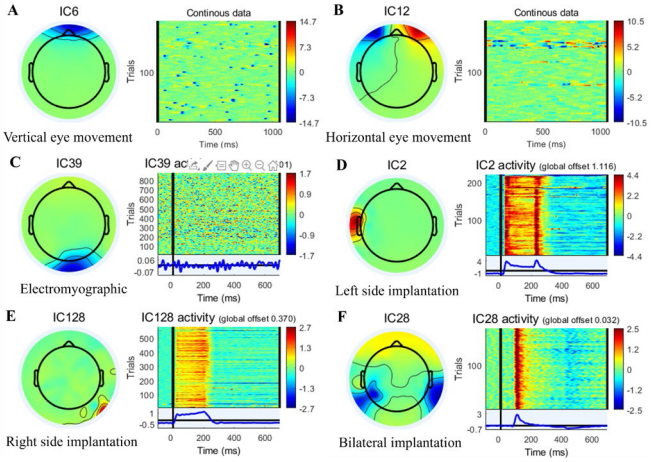

Fig. 3. Identification of ICs for Removal. (A) Vertical eye movement. (B) Horizontal eye Movement. (C) Electromyographic Noise. (D) Left-sided CI Artifact. (E) Right-sided CI Artifact. (F) Another Right-sided CI Artifact.

SVM integrates statistical theory with structural risk minimization principles to develop a model that classifies data based on sample attributes, renowned for its generalization ability. During the training phase, SVM employs features from each lead to construct a hyperplane that discriminates between CI-affected and unaffected vectors. In scenarios where the dataset is not linearly separable in finite-dimensional space, SVM maps the data to a higher-dimensional space. Here, a Gaussian radial basis function kernel defines the mapping, optimizing a maximum margin hyperplane in the expanded feature space to enhance the generalization error of the SVM. The careful selection of the penalty parameter c and the kernel function parameter γ is essential for shaping the hyperplane, with γ affecting its overall form and c determining error tolerance. To identify the optimal hyperparameters, a grid search was conducted, entailing an exhaustive exploration of various parameter combinations and their corresponding accuracies. This process involved defining a range for hyperparameters, dividing it into intervals, and systematically evaluating all possible values for each hyperparameter. Subsequent model training and testing for each parameter combination led to the selection of the optimal set. In this study, c was set to 10 and γ to 0.03, resulting in an optimal classification accuracy of 95.44%, as detailed in Table I. The model's results demonstrate robust identification and generalization capabilities for classifying CI-contaminated leads.

3) Automatic Removal of CI Low-Frequency Artifacts Using EEMD: Following the SVM classification of leads into CI-contaminated and uncontaminated categories, physiological artifacts such as EOG and EMG have been eliminated from the uncontaminated leads, as demonstrated in Figures 3A, 3B, and 3C. In the case of CI-contaminated leads, CI-related components are extracted using the EEMD combined with ICA algorithm. ICs identified by audiologists as exclusively comprising CI artifacts, devoid of physiological activity, are removed. ICs containing only CI artifacts are depicted in Figures 3D, 3E, and 3F. Analysis of CI artifact components reveals that unilateral implant recipients exhibit artifact activity

TABLE I
DATASET INFORMATION

ID	Age (m)	Age in activation (m)	Side	Implant brand	Implant model	Processor	ID	Age (m)	Age in activation (m)	Side	Implant brand	Implant model	Processor
1	57	14	L	AB	HiRes 90K	PSP	34	74	54	R	MED-EL	SONATAti100	OPUS1
2	21	18	R	MED-EL	PULSARci100	OPUS2	35	66	37	L	MED-EL	SONATAti100	OPUS2
3	20	14	R	AB	HiRes 90K	Naida Q90	36	37	18	L	MED-EL	Mi1000	OPUS2
4	30	27	R	AB	HiRes 90K	Harmony	37	77	45	L	MED-EL	SONATAti100	OPUS2
5	68	28	L	AB	HiRes 90K	Harmony	38	50	28	R	MED-EL	SONATAti100	OPUS2
6	20	19	R	MED-EL	SONATAti100	OPUS2	39	51	23	L	MED-EL	CONCERTO	OPUS1
7	28	28	BL	MED-EL	SONATAti100	OPUS2	40	34	30	BL	AB	HiRes 90K^{TM}	MS
8	71	70	R	MED-EL	SONATAti100	OPUS2	41	69	61	BL	MED-EL	SONATAti100	OPUS1
9	20	20	L	Cochlear	CI24RECA	CP910	42	82	52	R	MED-EL	CONCERTO	OPUS1
10	23	23	R	AB	HiRes 90K	Naida Q90	43	69	19	L	AB	HiRes 90K	Harmony
11	69	69	BL	AB	HiRes 90K	Naida Q90	44	42	42	BL	AB	HiRes 90K	Harmony
12	73	49	L	MED-EL	SONATAti100	OPUS2	45	67	17	L	AB	HiRes 90K	PSP
13	19	13	R	MED-EL	SONATAti100	OPUS2	46	52	30	L	Cochlear	CI512	CP910
14	71	18	R	AB	HiFocus Helix	Neptune	47	78	41	R	MED-EL	CONCERTO	OPUS2
15	33	18	R	AB	HiRes 90K	PSP	48	62	23	L	Cochlear	CI512	N6
16	23	10	R	AB	HiRes 90K	PSP	49	77	46	L	MED-EL	SONATAti100	OPUS2
17	35	34	L	MED-EL	Mi1000	OPUS2	50	42	34	L	MED-EL	Mi1000	OPUS2
18	52	28	R	MED-EL	SONATAti100	OPUS2	51	50	38	R	MED-EL	SONATAti100	OPUS2
19	72	30	R	AB	HiFocus1J	Harmony	52	43	9	R	MED-EL	CONCERTO	OPUS1
20	43	9	R	MED-EL	CONCERTO	OPUS1	53	67	26	L	MED-EL	SONATAti100	OPUS2
21	28	28	R	MED-EL	SONATAti100	OPUS2	54	41	39	BL	MED-EL	CONCERTO	OPUS2
22	77	26	BL	AB	HiFocus Helix	Neptune	55	30	27	R	AB	HiRes 90K	Harmony
23	26	25	BL	AB	HiRes 90K	Naida Q90	56	62	21	R	AB	HiRes 90K	Harmony
24	57	14	L	AB	HiRes 90K	PSP	57	30	15	R	AB	HiRes 90K	Harmony
25	68	28	L	AB	HiRes 90K	Harmony	58	51	18	L	MED-EL	SONATAti100	OPUS2
26	69	69	BL	AB	HiRes 90K	Naida Q90	59	51	17	R	Cochlear	CI512	CP910
27	73	49	L	MED-EL	SONATAti100	OPUS2	60	56	31	L	AB	HiRes 90K	Harmony
28	44	13	L	MED-EL	SONATAti100	OPUS2	61	51	20	L	MED-EL	SONATAti100	OPUS2
29	71	54	R	MED-EL	SONATAti100	OPUS1	62	41	37	R	MED-EL	SONATAti100	OPUS1
30	49	26	L	AB	HiRes 90K	Naida Q90	63	26	20	BL	MED-EL	SONATAti100	OPUS2
31	43	9	L	MED-EL	SONATAti100	OPUS1	64	38	8	L	MED-EL	SONATAti100	OPUS1
32	28	28	R	AB	HiRes 90K	Harmony	65	40	37	BL	MED-EL	CONCERTO	OPUS2
33	77	26	L	MED-EL	SONATAti100	OPUS2	66	28	28	R	MED-EL	SONATAti100	OPUS2

m means month; L means left; R means right; BL means bilateral

TABLE II
PERFORMANCE METRICS OF SVM CLASSIFICATION MODEL

Accuracy	ROC	Precision	Recall	F1
0.9544	0.9751	0.8277	0.9071	0.8656

predominantly on the implanted side, whereas bilateral implant recipients display artifacts distributed across bilateral temporal regions. Moreover, the time-series signal exhibits strong direct current (DC) artifacts and is extremely consistent across all trails. Here, we provide guidelines for ICs that can be removed during CI artifacts removal. Typically, CI artifacts are composed of two elements: high-frequency artifacts representing stimulus pulses, and DC or baseline artifacts [15], which exhibit a nonlinear time-varying relationship with pulse amplitude. Post band-pass filtering at 0.1-30Hz, the high-frequency CI artifacts are substantially reduced. However, DC artifacts persist in the EEG signal. Mere removal of ICs containing only CI artifacts is insufficient, as it leaves behind low-frequency DC artifacts. To mitigate this, the EEMD algorithm is applied to the signal, effectively diminishing CI noise.

EEMD represents an advancement of Empirical Mode Decomposition (EMD), a method that is data-driven, adaptive, and independent of prior assumptions, thus well-suited for analyzing nonlinear, non-stationary EEG data [26]. However, EMD is notably sensitive to noise and prone to mode mixing, potentially leading to inaccuracies in the derived Intrinsic Mode Functions (IMFs). EEMD effectively overcomes these limitations by providing a robust solution to the mode mixing issue [27]. EMD dynamically breaks down a multi-component signal into a series of band-limited IMFs, reflecting the signal's inherent time scale characteristics. Each IMF must satisfy two criteria: firstly, the count of local maxima or minima should be equal to or differ by no more than one from the number of zero-crossings; secondly, the mean value of the upper and lower envelopes, formed by these local extremes, should approximate zero. EEMD improves upon EMD by initially averaging the IMF set obtained from EMD decomposition, then introducing uniformly distributed white noise of the same standard deviation. This process effectively allocates various scale signal components to their corresponding scales in relation to the background noise, resulting in a refined IMF set. EEMD involves multiple iterations of applying EMD to the signal augmented with white noise. Given the distinct noise in each iteration and sufficient repetitions, the cumulative effect nullifies the added noise in the average, isolating the signal and minimizing mode mixing. For our study, we set the ensemble number for EEMD at 20 and the ratio of the standard deviation of the added Gaussian white noise to that of the original signal $s\,(t)$ at 0.1. The methodology involves:

(1) Add Gaussian white noise $w_k\,(t)$ to the original signal $s\,(t)$, forming a new signal $x_k\,(t)$

$$x_k\,(t) = s\,(t) + \varepsilon \cdot std\,(s\,(t)) \cdot w_k\,(t) \tag{1}$$

(2) Decompose the noisy signal $x_k\,(t)$with EMD to obtain m IMFs

$$x_k\,(t) = \sum_m c_{k,m}\,(t) \tag{2}$$

(3) Repeat steps (1) and (2) n times, adding white noise with each decomposition to obtain n sets of IMFs

(4) Utilize the principle that the statistical average of unrelated sequences is zero, average the IMFs, and obtain the final IMFs after EEMD decomposition.

$$c_m\,(t) = \frac{1}{n}\sum_{k=1}^{n} c_{k,m}\,(t) \tag{3}$$

Once the final IMFs are obtained from EEMD decomposition, we calculate the variance contribution rate, average period, and Pearson correlation coefficient for each IMF. This analysis assesses their relationship with the original sequence, retaining the IMFs with the top three indicator values to extract a signal free of CI artifacts. The EEG records, now devoid of both physiological and CI artifacts, from the two classified lead groups are then merged, culminating in a comprehensive, artifact-free whole-lead EEG dataset.

III. Result

In this section, the effectiveness of our artifact removal algorithm is evaluated using EEG data from both CI and their normal-hearing counterparts. We conduct qualitative comparisons, including analyses of time waveforms, Power Spectral Density (PSD) values before and after artifact removal, and Global Field Power (GFP), to assess the algorithm's ability to eliminate artifacts.

A. Reduction of CI Artifacts in ERPs

To illustrate the performance of our CI artifact reduction algorithm, we analyze full-head data across 128 channels, focusing on the distribution of CI artifacts. The data clearly show that CI artifacts are prevalent on the side where the implant is located. We also examine the algorithm's impact on the analysis of ERPs, which are derived by averaging EEG signals from 100 milliseconds before to 500 milliseconds after a stimulus. While band-pass filtering reduces high-frequency artifacts, low-frequency artifacts persist in the original signal, as depicted in the left panels of Figures 2A and 2B. The intensity of the recorded CI artifacts, as demonstrated in Figure 4A, follows a decay pattern emanating from the external device, indicating varying levels of contamination. Prior to the application of the artifact removal algorithm, the energy of the artifacts significantly exceeds that of the EEG components of interest. Brain topography maps reveal a concentration of high energy on the implant side, leading to distorted neural responses and implications for subsequent analyses.

Utilizing the SVM algorithm, data are segregated into two groups: channels affected by CI artifacts and those that are not. Channels free from CI contamination undergo routine preprocessing, which includes the elimination of physiological artifacts like eye and muscle movements (as illustrated in Figures 3A, 3B, and 3C). On the other hand, CI-affected channels are treated with our developed EEMD-ICA algorithm, initially targeting the removal of components exclusively composed of CI artifacts (shown in Figures 3D, 3E, and 3F). Despite this, some low-frequency CI artifacts persist, evident in the first row of Figure 5. The EEMD method involves introducing white noise and iteratively decomposing the signal via the EMD algorithm, producing a set of IMFs. An illustrative example in Figure 5 shows a channel automatically segmented into three IMFs. These IMFs and their corresponding decomposed signal are analyzed using three metrics: variance, average period, and Pearson correlation coefficient. The IMF exhibiting the highest metric values is retained. Post-EEMD processing effectively removes low-frequency CI artifacts, thereby optimally reconstructing the ERP components (as seen in the first row of Figure 5). Subsequently, the refined channels from both groups are amalgamated into a single dataset, depicted in Figure 4B. In the context of ERPs, this approach reduces CI artifacts while maximally preserving the components without energy loss. Brain topography maps, both pre- and post-artifact removal, exhibit a uniform distribution of outcomes.

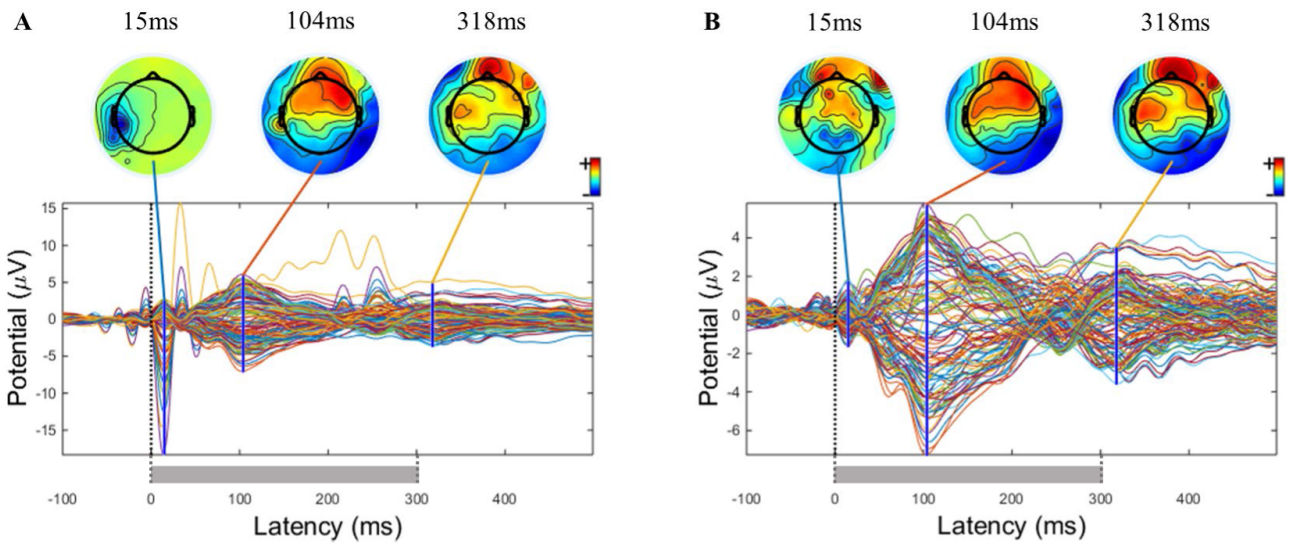

Fig. 4. Full-Lead ERP Comparison Pre and Post CI Artifact Removal. (A) Before Removal. (B) After Removal ERP Response.

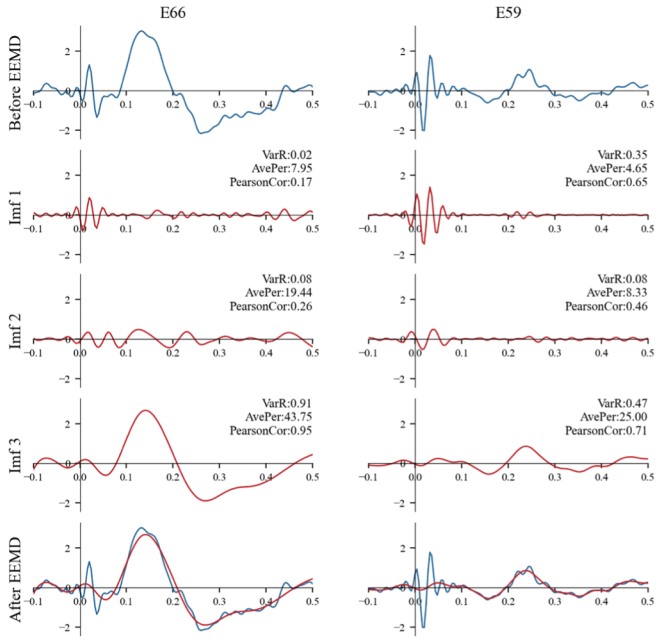

Fig. 5. EEMD Application on Channels with Residual Low-Frequency CI Artifacts. The top row visualizes the signal with residual low-frequency CI artifacts (blue line) subjected to EEMD. The following rows detail the EEMD decomposition process, yielding IMFs. Subsequent analysis involves calculating variance, average period, and Pearson correlation coefficients to assess the relationship between IMFs and the decomposed signal. The most significant three IMFs, indicated by the red line, are retained. The signal comparison before and after EEMD highlights the successful removal of CI artifacts and intact preservation of ERP components.

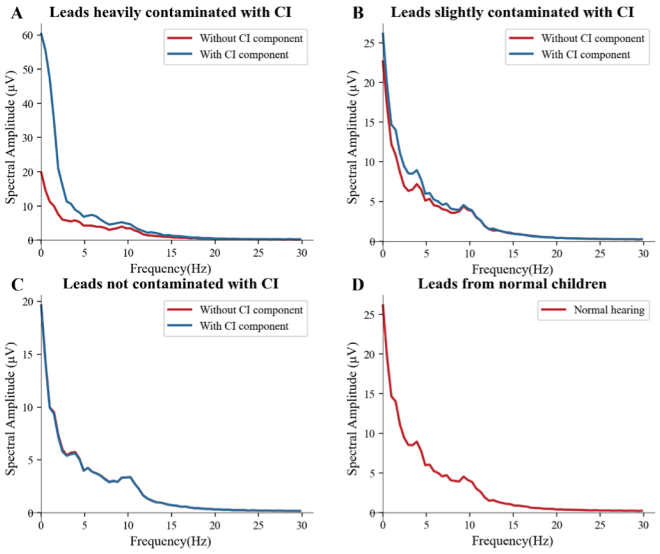

Fig. 6. PSD Analysis Pre and Post CI Artifact Removal. (A) Heavily CI Contaminated Channels. (B) Mildly CI Contaminated Channels. (C) Uncontaminated Channels. (D) PSD of Normal-Hearing Children. The post-removal algorithm significantly diminishes low-frequency range energy in heavily contaminated channels, with a minor reduction in mildly contaminated channels, while maintaining the original signal's frequency distribution. Uncontaminated channels' PSD remains unchanged post-removal. Corrected EEG recordings' PSD after CI artifact removal closely match those of normal-hearing peers.

B. Comparison of Time-Frequency-Space Domain Features in CI and Normal-Hearing Peers

In the frequency domain, our method demonstrates favorable outcomes. Figure 6 presents the PSD comparisons of EEG data, categorizing them into severely CI-contaminated, mildly CI-contaminated, non-contaminated, and post-correction EEGs, alongside the PSDs of normal-hearing children. The ideal outcome for the PSD of corrected EEG recordings is to minimize low-frequency CI artifacts while aligning closely with the PSD of the original EEG at other frequencies. In Figure 6, the PSD of the severely CI-contaminated EEG shows a notable reduction in the low-frequency range, while the mildly contaminated EEG exhibits a modest decrease. The PSD of the non-contaminated EEG remains stable before and after artifact removal. Comparing the PSD of corrected EEGs from CI with that of normal-hearing peers reveals a successful removal of low-frequency CI artifacts and a well-preserved brain activity below 20 Hz.

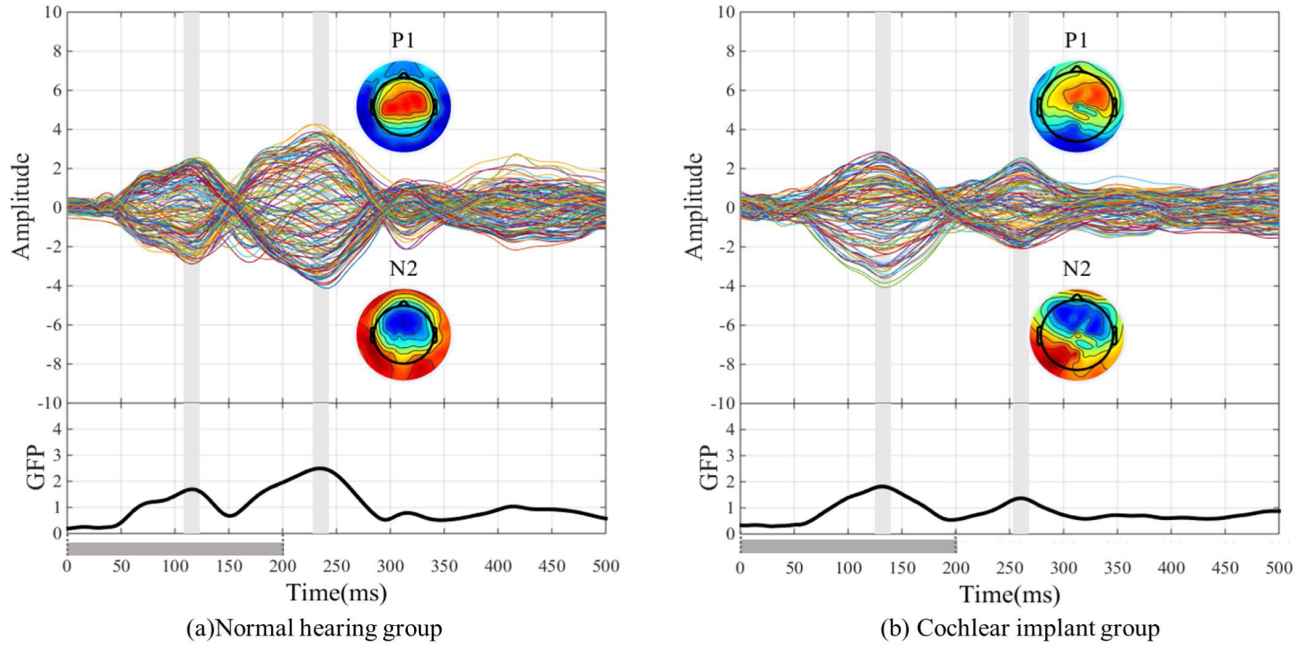

Fig. 7. Full-Lead ERP and Peak GFP Topographic Map Comparison. (a) Normal-Hearing Children Group. (b) Cochlear Implant Children Group. The figure presents topographic maps of full-lead ERP and peak GFP values for both groups. The CI group exhibits a clear reduction of low-frequency CI artifacts, and the spatial pattern at GFP peaks (P1, N2) aligns with normal-hearing children's distribution.

This indicates an effective full-head CI artifact elimination and optimal preservation of neural responses.

In terms of GFP, our method also demonstrates robust performance. GFP quantifies the standard deviation of voltage across all scalp electrodes at a specific moment, reflecting the brain's response to stimuli. Given prior evidence indicating that CI children demonstrate developmental ERP components comparable to their normal-hearing peers 24 months post-implantation, we compared the GFP of CI patients implanted for more than 24 months with age-matched normal-hearing individuals. Figure 7 displays topographic maps showcasing full-lead ERPs and peak GFP values for both groups. The analysis reveals that the full-lead average ERP components in the CI group are prominent, with low-frequency CI artifacts effectively minimized. Additionally, the spatial distribution of GFP peaks (notably at P1 and N2) aligns with that observed in normal-hearing peers, ensuring the integrity and reliability of the data for subsequent neuroplasticity research.

The shadow error plots of GFP depicted in Figure 8 affirm the efficacy of our method in consistently removing CI artifacts and accurately reinstating original neural responses at an individual level, underlining its widespread utility. Upon analyzing GFP peak data for both groups, the 100-200ms peak (P1) reveals no significant difference in latency or peak values between the groups (latency: F=1.396, P=0.272; peak: F=0.154, P=0.705). Conversely, the 200-300ms peak (N2a), often associated with the emergence of MMN, exhibits significant differences in latency (F=9.654, P=0.015) but not in peak values (F=2.059, P=0.189). These statistical findings reinforce the evidence found by prior research [21]. The P1 component, which represents the ability to hear sounds, developed to the same level as in normal peers, and the MMN component, which represents the ability to discriminate

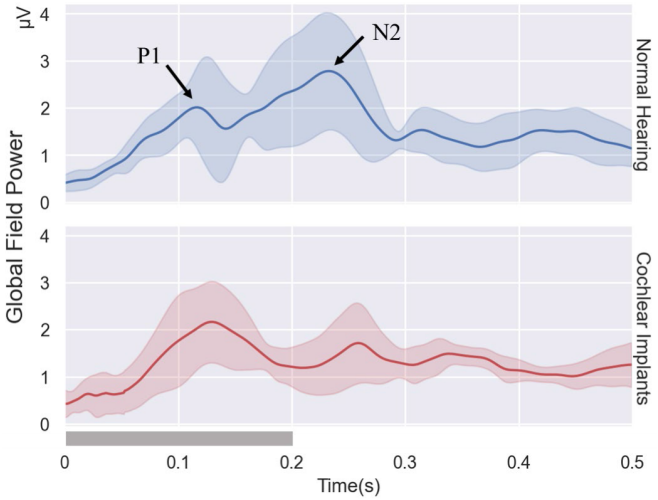

Fig. 8. GFP Shadow Error Plots for CI and Normal-Hearing Children. The GFP results for the CI children group show uniformity across subjects, effectively eliminating CI artifacts on an individual level and restoring authentic neural responses.

tones, remained at odds with normal peers 24 months after implantation. It attests to the method's substantial impact in eliminating CI artifacts and its effectiveness for neuroplasticity research.

IV. Discussion

This investigation presents a pioneering method for the removal of CI artifacts, explicitly designed for the objective evaluation of clinical auditory rehabilitation. This approach proficiently eradicates CI artifacts from all EEG leads, thereby advancing the clinical appraisal of auditory plasticity in CI recipients. It independently discerns channels tainted by

CI artifacts, obviating the need for prior knowledge. Utilizing a synergistic combination of EEMD and ICA, the method semi-automatically removes CI artifacts from affected channels. Acknowledging the variability among patients and the heterogeneity of CI coding strategies, the IC components of CI artifacts vary. Recognizing that numerous CI-related IC components are interwoven with neural activity, the study delineates guidelines to isolate IC components exclusively comprising CI artifacts, safeguarding against the obliteration or distortion of neural information in subsequent artifact removal phases.

From a methodological perspective, the removal of mixed CI artifacts from electroencephalogram (EEG) signals is a crucial step for subsequent EEG analyses, such as ERP analysis and source localization. However, previous methods, such as those relying solely on ICA, depend heavily on prior knowledge of specific artifact characteristics. CI artifacts often comprise as many as a dozen ICs, frequently intermingled with other elements, making their direct application in clinical auditory evaluations impractical. The method proposed in this article is data-driven. It begins by classifying channels based on whether they are contaminated by CI using a machine learning model, followed by artifact removal. The method does not advocate for the direct removal and interpolation of all leads contaminated by artifacts, as the number of leads affected by CI artifacts varies, and it is rare for only 1-2 electrodes to be impacted in EEG recordings. The employed EEMD-ICA approach ensures maximal preservation of neural responses throughout the artifact removal phase and attains superior performance in artifact removal tasks. The overall process of this method is non-prior and adaptive, offering a novel way to eliminate CI artifacts. Particularly, based on a real EEG dataset with CI, this method demonstrates robust capabilities in handling CI artifacts. The data processed using this method demonstrate significant differences in the latency of evoked responses based on the type of auditory stimulus. Homogeneity of variance tests were conducted on the data from the three auditory stimulus groups, followed by one-way ANOVA and multiple comparison corrections. The results indicate significant differences in P1 latency between pure tones and syllables ($P = 0.001$) as well as between pure tones and tones ($P = 0.001$). Furthermore, the MMN latency for pure tones was significantly different from that for tones ($P = 0.019$). Multiple regression analysis also suggests a positive correlation between the difficulty of auditory stimuli and both P1 latency ($t = 4.585$, $P < 0.001$) and MMN latency ($t = 3.781$, $P = 0.001$). These statistical results suggest that this method can be an effective tool for exploring changes in neural activity following cochlear implantation.

From an application standpoint, compared to previous methods that relied on prior knowledge for analysis, this method offers a universal guideline for processing EEGs of CI under different auditory stimuli. This flexibility holds great potential for EEG to objectively assess different auditory abilities in the clinic. Its use is not limited to ERP analysis, clinical assessments can reliably analyze auditory plasticity in CI users, greatly promoting the clinical application of auditory brain-computer interfaces. Furthermore, for a comprehensive evaluation of this method, it should be evaluated on an expansive dataset of CI EEG recordings, encompassing a variety of distinct tasks.

Additionally, it is important to acknowledge the limitations of our work. This study employs a supervised machine learning model, whose training process requires a large amount of expert-annotated data. Although the artifact removal stage is non-prior, given that the field of CI artifact elimination in CI-EEG is still nascent, using expert-annotated datasets for more extensive validation is crucial. An unsupervised machine learning model is also a future direction for our research. Moreover, this study provides a guideline for removing ICs that solely comprise CI artifacts. Although the method can be directly utilized by non-experts, removing ICs presently requires manual execution. To achieve automated IC removal, experts must label the ICs based on the characteristics of time series, PSD, and topographical maps, thereby developing an automated model for the elimination of CI-related ICs. Furthermore, deep learning approaches surpass models developed through manual feature extraction. Simulating expert annotation of CI-related ICs, informed by techniques employed in other artifact removal study (e.g. automated EOG artifact removal), is posited as a goal for advancing CI artifact removal.

V. Conclusion

Artifact removal is a critical aspect of EEG analysis. This is particularly pertinent in the objective evaluation of auditory rehabilitation for CI users. The incompatibility of CIs with MRI presents unique challenges in assessing brain activity during the rehabilitation process. Therefore, the effective removal of CI artifacts is essential for accurate analyses of brain plasticity. In this study, we introduced a semi-automated CI artifact removal approach, specifically designed for clinical auditory rehabilitation evaluations, establishes guidelines for its manual aspects, and demonstrates its superiority in removing artifacts across whole-head EEG signals. This method is designed to be user-friendly for non-experts and adeptly maintains the integrity of neural signals of interest during the artifact removal process. Consequently, it serves as a potent tool for integrating auditory brain-computer interfaces into the clinical evaluation of CI auditory rehabilitation.

Acknowledgment

The authors are very grateful to Dr. Jin Yin for her suggestions on the performance evaluation of the algorithms.

References

[1] B. S. Wilson, D. L. Tucci, M. H. Merson, and G. M. O'Donoghue, "Global hearing health care: New findings and perspectives," *Lancet*, vol. 390, no. 10111, pp. 2503–2515, Dec. 2017.

[2] E. Saunders et al., "Threshold, comfortable level and impedance changes as a function of electrode-modiolar distance," *Ear Hearing*, vol. 23, pp. 2–8, Feb. 2002.

[3] T. Green, A. Faulkner, and S. Rosen, "Spectral and temporal cues to pitch in noise-excited vocoder simulations of continuous-interleaved-sampling cochlear implants," *J. Acoust. Soc. Amer.*, vol. 112, no. 5, pp. 2155–2164, Nov. 2002.

[4] L. M. Friesen, R. V. Shannon, D. Baskent, and X. Wang, "Speech recognition in noise as a function of the number of spectral channels: Comparison of acoustic hearing and cochlear implants," *J. Acoust. Soc. Amer.*, vol. 110, no. 2, pp. 1150–1163, Aug. 2001.

[5] S. S. Shushtari et al., "Development and psychometric evaluation of the Persian version of the phoneme recognition test a central auditory processing measure," *Iran. J. Child. Neurol.*, vol. 16, no. 3, pp. 79–93, Jul. 2022.

[6] I. Boisvert, M. Reis, A. Au, R. Cowan, and R. C. Dowell, "Cochlear implantation outcomes in adults: A scoping review," *PLoS ONE*, vol. 15, no. 5, May 2020, Art. no. e0232421.

[7] N. Kraus et al., "The mismatch negativity cortical evoked potential elicited by speech in cochlear-implant users," *Hearing Res.*, vol. 65, nos. 1–2, pp. 118–124, Feb. 1993.

[8] A. Sharma, M. F. Dorman, and A. Kral, "The influence of a sensitive period on central auditory development in children with unilateral and bilateral cochlear implants," *Hearing Res.*, vol. 203, nos. 1–2, pp. 134–143, May 2005.

[9] K. Mehta, M. Mahon, P. Watkin, J. Marriage, and D. Vickers, "A qualitative review of parents' perspectives on the value of CAEP recording in influencing their acceptance of hearing devices for their child," *Int. J. Audiol.*, vol. 58, no. 7, pp. 401–407, Jul. 2019.

[10] B. Intartaglia, A. G. Zeitnouni, and A. Lehmann, "Recording EEG in cochlear implant users: Guidelines for experimental design and data analysis for optimizing signal quality and minimizing artifacts," *J. Neurosci. Methods*, vol. 375, Jun. 2022, Art. no. 109592.

[11] P. M. Gilley, A. Sharma, M. Dorman, C. C. Finley, A. S. Panch, and K. Martin, "Minimization of cochlear implant stimulus artifact in cortical auditory evoked potentials," *Clin. Neurophysiol.*, vol. 117, no. 8, pp. 1772–1782, Aug. 2006.

[12] A. Presacco, H. Innes-Brown, M. J. Goupell, and S. Anderson, "Effects of stimulus duration on event-related potentials recorded from cochlear-implant users," *Ear Hearing*, vol. 38, no. 6, pp. e389–e393, Nov. 2017.

[13] P. W. Bauer, A. Sharma, K. Martin, and M. Dorman, "Central auditory development in children with bilateral cochlear implants," *Arch. Otolaryngol.-Head Neck Surg.*, vol. 132, no. 10, p. 1133, Oct. 2006.

[14] M. Hofmann and J. Wouters, "Electrically evoked auditory steady state responses in cochlear implant users," *J. Assoc. Res. Otolaryngol.*, vol. 11, no. 2, pp. 267–282, Jun. 2010.

[15] M. Mc Laughlin, A. L. Valdes, R. B. Reilly, and F.-G. Zeng, "Cochlear implant artifact attenuation in late auditory evoked potentials: A single channel approach," *Hearing Res.*, vol. 302, pp. 84–95, Aug. 2013.

[16] G. BinKhamis, E. Perugia, M. O'Driscoll, and K. Kluk, "Speech-ABRs in cochlear implant recipients: Feasibility study," *Int. J. Audiology*, vol. 58, no. 10, pp. 678–684, Oct. 2019.

[17] P. Comon, "Independent component analysis, a new concept?" *Signal Process.*, vol. 36, no. 3, pp. 287–314, Apr. 1994.

[18] O. Dimigen, "Optimizing the ICA-based removal of ocular EEG artifacts from free viewing experiments," *NeuroImage*, vol. 207, Feb. 2020, Art. no. 116117.

[19] Y. Song and F. Sepulveda, "A novel technique for selecting EMG-contaminated EEG channels in self-paced brain–computer interface task onset," *IEEE Trans. Neural Syst. Rehabil. Eng.*, vol. 26, no. 7, pp. 1353–1362, Jul. 2018.

[20] H. Deprez, R. Gransier, M. Hofmann, A. van Wieringen, J. Wouters, and M. Moonen, "Independent component analysis for cochlear implant artifacts attenuation from electrically evoked auditory steady-state response measurements," *J. Neural Eng.*, vol. 15, no. 1, Feb. 2018, Art. no. 016006.

[21] G. Ni et al., "Objective electroencephalography-based assessment for auditory rehabilitation of pediatric cochlear implant users," *Hearing Res.*, vol. 404, May 2021, Art. no. 108211.

[22] F. Mina, V. Attina, Y. Duroc, E. Veuillet, E. Truy, and H. Thai-Van, "Auditory steady state responses and cochlear implants: Modeling the artifact-response mixture in the perspective of denoising," *PLoS ONE*, vol. 12, no. 3, Mar. 2017, Art. no. e0174462.

[23] V. Attina et al., "A new method to test the efficiency of cochlear implant artifacts removal from auditory evoked potentials," *IEEE Trans. Neural Syst. Rehabil. Eng.*, vol. 25, no. 12, pp. 2453–2460, Dec. 2017.

[24] L. Wagner, N. Maurits, B. Maat, D. Baskent, and A. E. Wagner, "The cochlear implant EEG artifact recorded from an artificial brain for complex acoustic stimuli," *IEEE Trans. Neural Syst. Rehabil. Eng.*, vol. 26, no. 2, pp. 392–399, Feb. 2018.

[25] R. Gransier, F. Guérit, R. P. Carlyon, and J. Wouters, "Frequency following responses and rate change complexes in cochlear implant users," *Hearing Res.*, vol. 404, May 2021, Art. no. 108200.

[26] N. E. Huang et al., "The empirical mode decomposition and the Hilbert spectrum for nonlinear and non-stationary time series analysis," *Proc. Roy. Soc. London. Ser. A, Math., Phys. Eng. Sci.*, vol. 454, no. 1971, pp. 903–995, Mar. 1998.

[27] Z. Wu and N. E. Huang, "Ensemble empirical mode decomposition: A noise-assisted data analysis method," *Adv. Adapt. Data Anal.*, vol. 1, no. 1, pp. 1–41, Jan. 2009.